JAERI-M
86-075

EXPERIMENTAL STUDY OF FILM BOILING HEAT TRANSFER IN STEAM-WATER TWO-PHASE FLOW

May 1986

Takamichi IWAMURA

日本原子力研究所
Japan Atomic Energy Research Institute

JAERI-Mレポートは，日本原子力研究所が不定期に公刊している研究報告書です。
入手の問合わせは，日本原子力研究所技術情報部情報資料課（〒319-11茨城県那珂郡東海村）あて，お申しこしください。なお，このほかに財団法人原子力弘済会資料センター（〒319-11 茨城県那珂郡東海村日本原子力研究所内）で複写による実費頒布をおこなっております。

JAERI-M reports are issued irregularly.
Inquiries about availability of the reports should be addressed to Information Division Department of Technical Information, Japan Atomic Energy Research Institute, Tokai-mura, Naka-gun, Ibaraki-ken 319-11, Japan.

編集兼発行　日本原子力研究所
印　　刷　㈱高野高速印刷

Experimental Study of Film Boiling Heat Transfer in Steam-Water Two-Phase Flow

Takamichi IWAMURA

Department of Reactor Safety Research
Tokai Research Establishment
Japan Atomic Energy Research Institute
Tokai-mura, Naka-gun, Ibaraki-ken

(Received April 22, 1986)

A steady-state film boiling experiment at void fractions between 0.6 and 0.95 was performed to investigate the film boiling heat transfer coefficient in dispersed flow and transition regions during the reflood phase of a PWR-LOCA. The film boiling heat transfer in these regions was assumed to be superimposed by three different mechanisms; radiation, forced convection to steam and droplet impingement on wall. The radiation and forced convection heat transfer coefficients were evaluated by using the Stefan-Boltzmann equation and the Dittus-Boelter equation, respectively. The thermodynamic non-equilibrium was taken into account in the forced convection heat transfer mode. A new correlation for the heat transfer coefficient due to droplet impingement was derived from the dispersed flow heat transfer model developed by Forslund and Rohsenow. The correlation is a function of steam and water velocities, void fraction, fluid properties and wall superheat. The agreement between calculated and experimentally derived heat transfer coefficients was fairly good for the present experiment.

Keywords: Film Boiling Heat Transfer, Two-Phase Flow, Reflood, LOCA, Radiation, Forced Convection, Droplets Impingement, Thermal Non-equilibrium, Post CHF Heat Transfer, Dispersed Flow

蒸気－水二相流中での膜沸騰熱伝達実験

日本原子力研究所東海研究所原子炉安全工学部
岩　村　公　道

（１９８６年４月２２日受理）

PWR－LOCA時再冠水過程において見られる液滴分散流及び遷移流領域における膜沸騰熱伝達率を調べるため，0.6から0.95のボイド率範囲において定常膜沸騰実験を実施した。この領域内での膜沸騰熱伝達は，熱輻射，蒸気強制対流及び加熱面への液滴衝突の３種類のメカニズムが重畳しているものと考えられる。輻射及び強制対流熱伝達率は，それぞれStefan－Boltzmannの式とDittus－Boelterの式により評価した。強制対流熱伝達モードでは熱力学的非平衡を考慮した。液滴衝突による熱伝達率については，Forslund－Rohsenowのモデルに基づいて新しい相関式を導出した。本相関式は，蒸気と水の流速，ボイド率，流体物性値及び壁面過熱度の関数である。本相関式は，実験により求めた熱伝達率と良い一致を示した。

東海研究所：〒３１９－１１茨城県那珂郡東海村白方字白根２－４

Contents

目　　次

List of Tables

List of Figures

1. Introduction

Film boiling heat transfer under forced convection two-phase flow governs the cladding temperature transient during the reflood phase of a loss-of-coolant accident (LOCA) in a pressurized water reactor (PWR). A number of experimental and theoretical studies have been carried out for the forced convection film boiling and a lot of correlations have been proposed. Chen et al.[1], reviewed several correlations based on equilibrium and non-equilibrium models.

During the reflood phase, the film boiling heat transfer is observed in three different flow regimes; inverted annular flow, dispersed flow, and transition flow between these two flow regimes. Several correlations have been proposed for each of these flow regimes. Bromley type correlations are generally used for the inverted annular flow regime. For example, the Murao-Sugimoto's correlation[2] which is used in REFLA code[3] is in fairly good agreement with the data from a small scale reflood experiment and FLECHT experiments.

However, the boundary void fractions among these three flow regimes are differen in different codes. For example, in the COBRA/TRAC code[4], inverted annular film boiling is selected when the void fraction is less than 0.6 and dispersed flow film boiling is selected when the void fraction is greater than 0.8. At intermediate void fractions between 0.6 and 0.8, the heat flux is interpolated between the values for inverted annular and dispersed flow film boiling because there is no reliable heat transfer correlation for the transition flow regime. On the other hand, it was indicated in the reflood tests with Slab Core Test Facility (SCTF) that the void fraction during the important period of the reflood phase ranged between 0.6 and 0.95[5]. Therefore, it is necessary to develope a new film boiling correlation especially in the transition and dispersed flow regimes.

The purpose of the present study is to investigate the film boiling heat transfer coefficient at the void fractions between 0.6 and 0.95 by performing a steady-state film boiling experiment. In the present study, emphasis is placed on the effects of local flow parameters such as steam velocity, water velocity and void fraction on the film boiling heat transfer coefficient. The film boiling heat transfer coefficient in these void fraction ranges is assumed to be a sum of three components; radiation, forced convection to steam, and droplets impingement on

heated surface. The heat transfer coefficients due to radiation and steam forced convection are estimated from the experimental data. Then the remaining heat transfer coefficient, which is obtained by subtracting the above two heat transfer coefficients from the total one, is correlated with the steam and water velocities and void fraction. The flow pattern in the test section is also discussed based on the observation results.

2. Experimental Apparatus

A schematic diagram of the experimental apparatus used for the steady-state film boiling experiment is shown in Fig. 2.1. The main part of the apparatus consists of an annular test section, a saturation water supply system, a steam supply system and a steam/water separator. Transient boiling experiment loop[6] was used to heat up the water in the loop.

2.1 Heater Rod

The test section is a vertically oriented annulus as shown in Fig. 2.2. The inner heater rod is composed of three regions; heated region made of Inconnel 600 and upper and bottom non-heated regions made of Copper. These Copper tubes are welded to the Inconnel tube through Nickel tubes for better welding. The top and bottom Copper regions are connected to electrodes, respectively. The heater rod is directly heated by a direct current. The maximum heating power used in this experiment was 7.4 kW (667 A and 11.1 volt).

The outer diameter and the length of the heated region are 15.9 mm and 800 mm, respectively. The thickness of the heated region is 1.3 mm for the middle 735 mm and bottom 5 mm. In order to suppress the quench front propagation from the bottom and the top part of the heater rod, the heat flux is increased from 5 to 45 mm and from 780 to 800 mm from the bottom of heated part by reducing the tube thickness to 0.8 mm and 1.0 mm, respectively.

Eight Chromel-Alumel (C/A) un-grounded sheath thermocouples are embedded in the heater tube from the inside to measure the heater rod temperature. The sheath diameters are 1.6 mm for the top and bottom thermocouples (TC 1 and TC 8) and 0.5 mm for the other six thermocouples (TC 2 through TC 7). Based on X-ray photographs, the Chromel-Alumel junction is estimated to be located at approximately 0.7 mm from the outer surface of the heater rod for TC 2 through TC 7. The thermocouple sheaths are isolated from the heater rod using ceramic sleeves inside the heater rod. Magnesium oxide (MgO) powder is packed closely inside the heater rod so as to increase the heat capacity of the rod.

The heater rod penetrates through the bottom lid. Two O-rings are used to seal the penetration part and also to relieve the thermal expansion of the heater rod.

2.2 Flow Shroud

Two kinds of flow shrouds were provided; a stainless-steel tube and a glass tube. The inner diameter of these two flow shrouds is 34 mm and therefore the flow area and the hydraulic diameter are 0.000709 m^2 and 0.0181 m, respectively. As shown in Fig. 2.2, three pressure taps and four fluid temperature C/A thermocouples (1.6 mm ϕ) were provided at the stainless-steel shroud so as to measure the local void fractions and fluid temperatures along the test section, respectively. On the other hand, the glass tube was used to observe the two-phase flow behavior during the film boiling experiment. A high speed video camera and a 35 mm camera were used to take pictures of the flow pattern.

The fluid temperatures at the inlet and outlet of the test section were also measured with C/A thermocouples.

2.3 Water and Steam Supply Systems

Saturated water and steam are injected into the lower plenum through the water and steam injection nozzles, respectively, as shown in Fig. 2.2. The flow rates of water and steam can be independently controlled to establish proper test conditions of water and steam velocities and void fraction.

The saturation water supply system consists of a saturation water tank, a pressurized nitrogen gas system, two flow meters and two flow control valves. The water is injected by the nitrogen pressure. The flow rate is kept at a constant value by manually operating the flow control valves during the experiment.

Steam is additionally injected into the test section at a constant flow rate. The steam is supplied from an outside boiler with the maximum pressure of 0.6 MPa. In order to supply the steam uniformly into the test section, four steam injection nozzles are used as shown in Fig. 2.3.

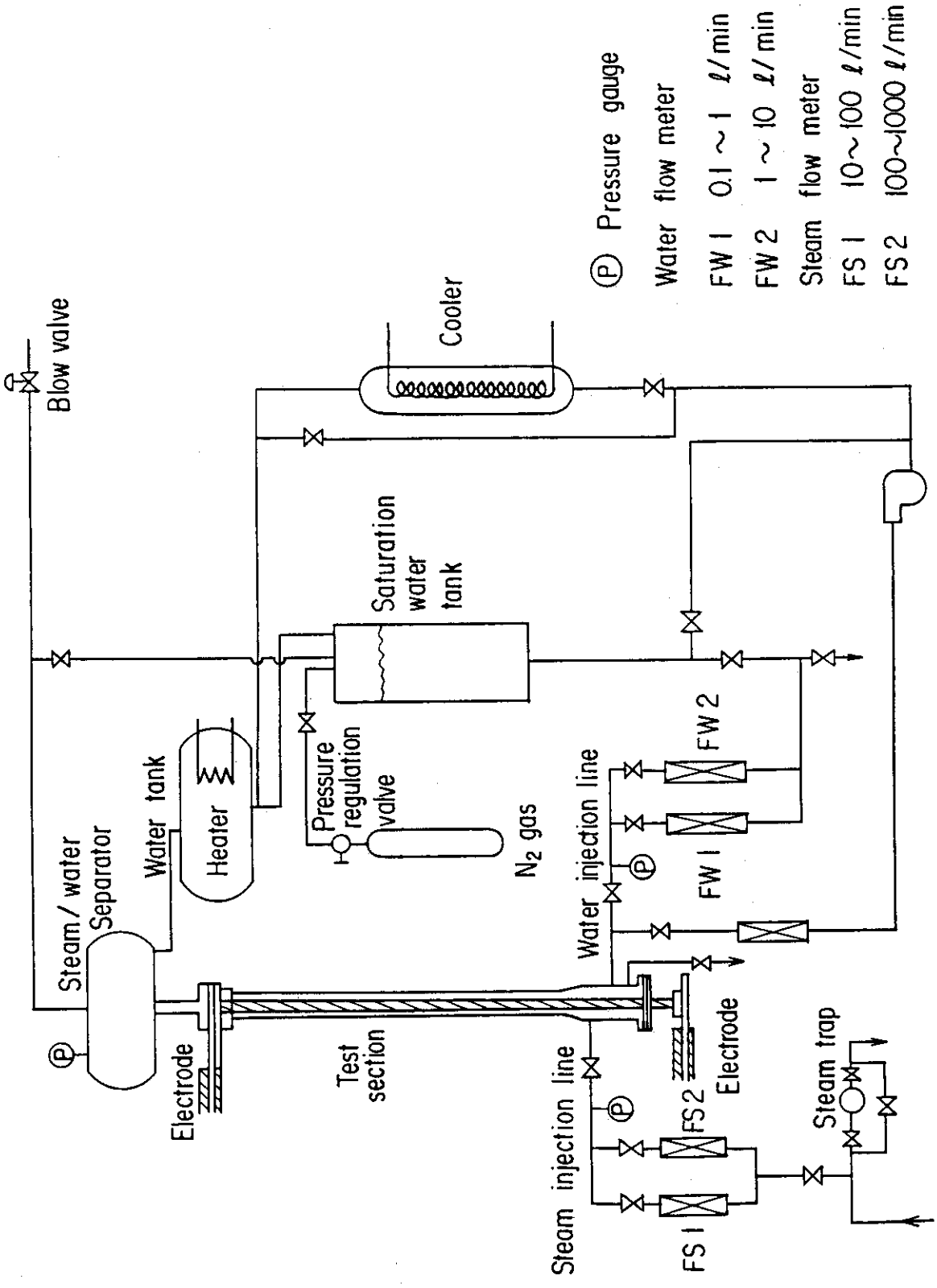

Fig. 2.1 Schematic diagram of film boiling experimental apparatus

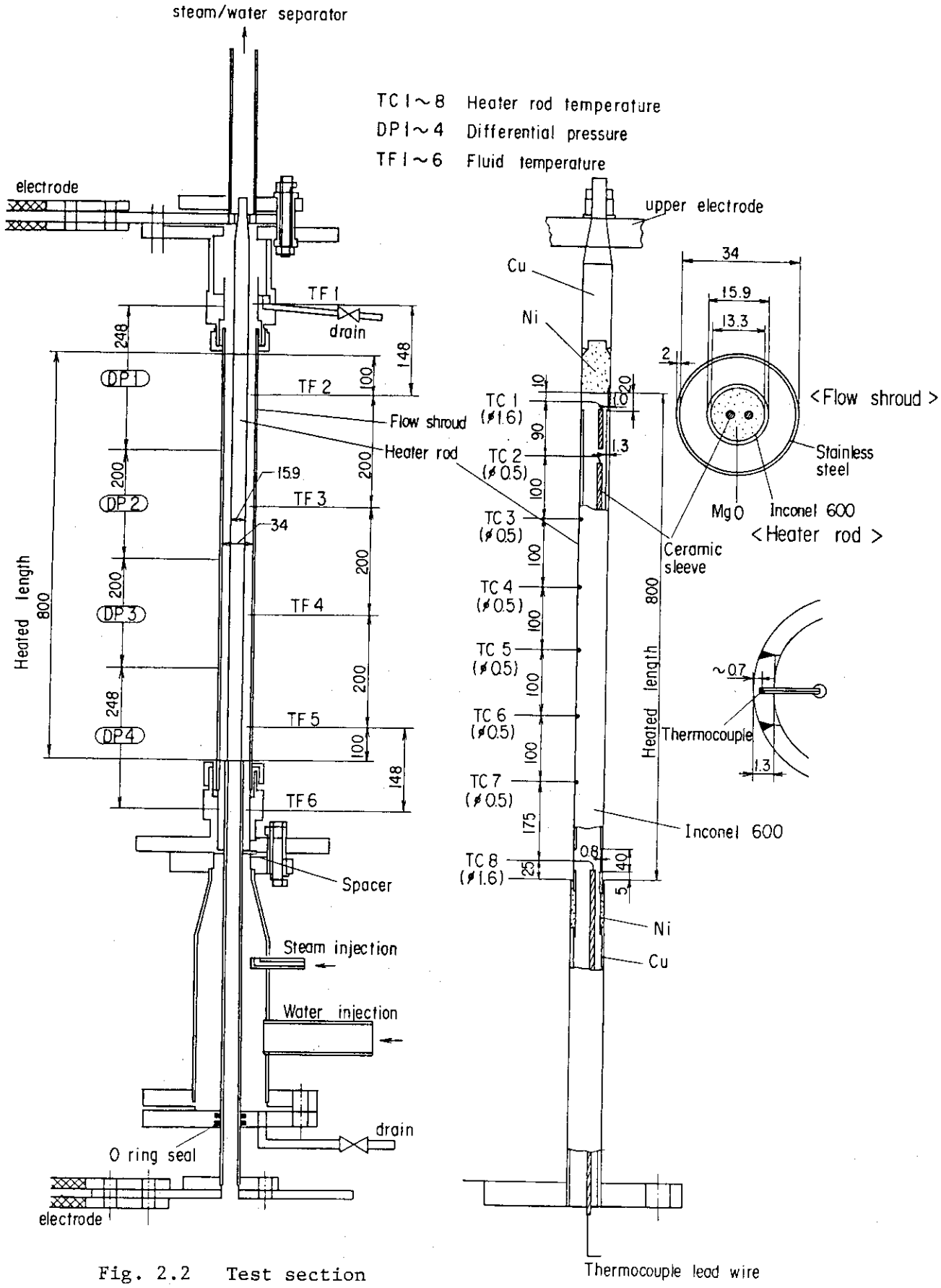

Fig. 2.2 Test section

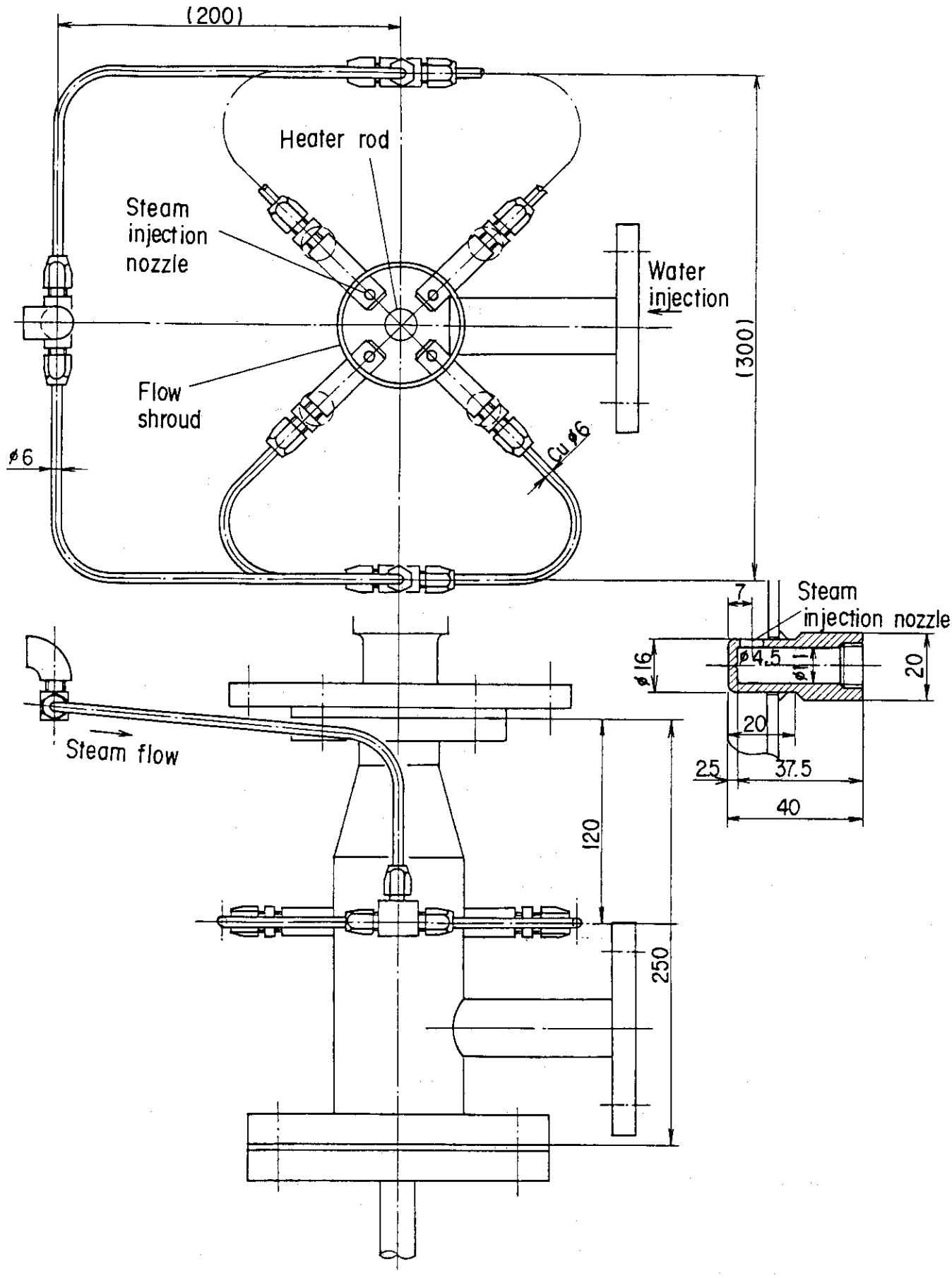

Fig. 2.3 Steam injection nozzles

3. Test Conditions, Test Procedure and Date Reduction

3.1 Test Conditions

The present film boiling experiments were performed under the conditions simulating the reflood phase of a PWR-LOCA. The test conditions are listed in Table 3.1.

3.2 Test Procedure

The test procedure for the steady-state film boiling heat transfer experiment is as follows: At first, the water circulating in the transient boiling experiment loop was heated up to the saturation temperature at about 0.3 MPa using the test section heater. Then, the saturation water tank was filled with the saturation water and thereafter the tank was isolated from the loop to be pressurized by nitrogen gas up to about 0.6 MPa. After warming the steam and water injection lines, the water in the test section was drained and the steam injection into the test section began at a constant flow rate. Next, the heater rod power was turned on to increase the heater rod temperature. When the heater rod temperature exceeded about 973 K, the saturation water injection was initiated at a constant flow rate. The steam and water flow rates were controlled manually during the test period so as to keep these flow rates at given values, respectively. In order to establish a steady-state condition under given steam and water flow rates, the heater rod power was delicately controlled to maintain the heater rod at a constant temperature for more than 70 s. After equilibrating the heating power with the heat flux into the steam-water two-phase flow, the rod temperatures, the fluid temperatures, and the differential pressures were recorded on multi-pen recorders.

3.3 Calculation of Heat Transfer Coefficient

3.3.1 Steady-State Assumption

The heat transfer coefficient in the present experiment was obtained from the assumption of steady-state condition. That is, the heater rod temperature profile was kept constant with respect to time. The transient temperature profile can be calculated from the transient heat conduction equation. Heisler[7] presented a convenient chart to give the temperature transient in an infinite plate under a sudden change

of surface temperature as a function of Fourier number, F_o, and Biot number, B_i. These two dimensionless parameters are defined as

$$F_o = \frac{at}{\ell^2} \tag{3-1}$$

and

$$B_i = \frac{h\ell}{k_w} \quad . \tag{3-2}$$

In the present experiment, the film boiling heat transfer coefficient is estimated to be between 200 and 300 $W/m^2 \cdot K$. Therefore, by introducing the thermal conductivity of Inconnel 600 at about 1000 K and the heater tube thickness into eqs. (3-2), the $1/B_i$ of the heater rod is estimated to range between 60 and 100. Based on the Heisler's chart, the temperature in an infinite plate reaches 90 % of the final value at the F_o of 140 and 225 corresponding to the $1/B_i$ of 60 and 100, respectively. The corresponding times obtained from eq. (3-1) are 45.2 and 72.7 s, respectively. Therefore, in order to apply the steady-state assumption to the heat transfer calculation, the continuating time at a constant temperature should be more than 70 s. Most of the present heat transfer data were obtained under the continuating time more than 120 s.

3.3.2 Heat Transfer Coefficient under Steady-State Condition

As discussed in the previous section, if the heater rod temperature is kept at a constant value for more than 70 s, the temperature profile in the heater rod can be assumed to be in a steady-state condition and therefore the heat transfer coefficient can be obtained from the measured heater rod temperature using the steady-state heat conduction equation.

The steady-state heat conduction equation in a cylindrical geometry is written as

$$k_w \frac{1}{r} \frac{d}{dr} \left(r \frac{dT}{dr} \right) + q''' = 0 \quad . \tag{3-3}$$

The boundary conditions are

$$\left(\frac{\partial T}{\partial r} \right)_{r=r_1} = 0 \quad , \tag{3-4}$$

$$(T)_{r=r_M} = T_M \ . \tag{3-5}$$

The geometry of heater tube is illustrated in Fig. 3.1 for the heat transfer calculation.

The heater rod surface temperature and the heater rod surface heat flux are obtained by solving eq. (3-3) under the boundary conditions of eqs. (3-4) and (3-5). The results are;

$$T_W = T_M - \frac{q'''}{2k_w} r_1^2 \ln \frac{r_M}{r_2} + \frac{q'''}{4k_w}(r_M^2 - r_2^2) \tag{3-6}$$

and

$$q'' = -k_w \left(\frac{\partial T}{\partial r} \right)_{r=r_2} = \frac{q''' (r_2^2 - r_1^2)}{2 r_2} \ . \tag{3-7}$$

Since the thickness of the heater tube is varied as shown in Fig. 3.1, the heating voltage for the heated length with 1.3 mm thickness is reduced to 0.8934 times the measured voltage for the total heater rod. Consequently, the heat generation rate in the heater rod with 1.3 mm thickness is expressed in terms of the measured voltage and current as

$$q''' = \frac{0.8934 \ V_M \ I_M}{\frac{\pi}{4} (15.9^2 - 13.3^2) \times 10^{-6} \times 0.74} = 2.025 \times 10^4 \ V_M \ I_M \tag{3-8}$$

From eqs. (3-6), (3-7) and (3-8), the heat transfer coefficient from the heater rod surface to the fluid is given by

$$h = \frac{q''}{T_w - T_{sat}} = \frac{24.17 \ V_M \ I_M}{T_M - T_{sat} - \frac{0.0126}{k_w} V_M \ I_M} \tag{3-9}$$

3.4 Void Fraction

Void fractions at four elevations were calculated from the corresponding measured vertical differential pressures by neglecting the effects of frictional and accelerational pressure drops as follows;

$$\alpha_i = 1 - \frac{1000 \ \Delta P_i}{\rho_\ell \ L_i} \qquad i = 1 \sim 3, \text{ where } \Delta P_i \ (\text{mm } H_2O) \tag{3-10}$$

The local void fractions at the thermocouple elevations from 300 to 700 mm from the bottom of the heated part were obtained by interpolating the measured void fractions using a parabolic function. The

differential pressure data from DP4 was not used for the void fraction calculation because the quench front was within the measurement span of DP4, suggesting that the differential pressure along this span did not indicate the local void fraction.

3.5 Superheated Steam Temperature and Actual Quality

The steam in the dispersed film boiling region is considered to be superheated to some degrees. In this case, the actual quality should be less than the thermal equilibrium quality. The fluid temperature data in the present experiment indicated that the steam superheat of more than 100 K existed in the test section. However, it is extreamly difficult to measure the correct superheated steam temperature because the measured temperature is affected by the liquid droplets impinging on the thermocouple. Since the actual steam temperature is essential to evaluate the heat transfer coefficient due to steam forced convection, several calculation methods have been proposed to estimate the superheated steam temperature. In the present study, the Chen's correlation[1] for thermodynamic non-equilibrium was adopted because most of the experimental ranges used to develope the correlation involve the present experimental ranges except the geometry and system pressure as shown in Table 3.2.

Based on the Chen's model, the ratio between the actual quality and the equilibrium quality is given by

$$\frac{X_a}{X_e} = 1 - B(P)\,\frac{T_g - T_{sat}}{T_w - T_g} \tag{3-11}$$

where $$B(P) = \frac{0.26}{1.15 - (P/Pc)^{0.65}}$$

The heat balance gives the relation of

$$\frac{X_a}{X_e} = \frac{H_{fg}}{H_g - H_e} = \frac{H_{fg}}{H_{fg} + C_{pg}(T_g - T_{sat})} \tag{3-12}$$

The superheated steam temperature, T_g, and the ratio between actual quality and equilibrium quality, X_a/X_e, can be obtained by solving equations (3-11) and (3-12) simultaneously. Then, the T_g is expressed as

$$T_g = \frac{C_{pg}\,T_w - B(P)(H_{fg} - C_{pg}\,T_{sat})}{C_{pg}(1 + B(P))} \tag{3-13}$$

The C_{pg} in eq. (3-13) is evaluated at the film temperature given by

$$T_f = \frac{T_w + T_g}{2} \tag{3-14}$$

The other thermal properties of superheated steam used in the heat transfer calculation are also evaluated at the film temperature.

Since the Chen's empirical correlation was based on the data from tube geometry, the superheated steam temperature calculated by eq. (3-13) is considered to be overestimated in the present annular test section because the surface temperature at the outer tube is approximately equal to the saturation temperature. In the present study, the steam temperature was varied from the saturation temperature to the superheated steam temperature given by eq. (3-13) so as to evaluate the effect of uncertainty involved in the estimation of steam temperature.

3.6 Steam and Water Velocities

The local steam and water velocities at the thermocouple elevations were calculated by a one-dimensional steady-state mass balance method considering the superheat of steam. In this calculation, the water accumulation rate was neglected because the bottom and top quench propagation velocities were less than 1 mm/s in most cases. Based on this steady-state assumption, the total flow rate is given by

$$W_T = W_{go} + W_{\ell o} = W_{gj} + W_{\ell j}, \quad j = 1 \sim 8 \tag{3-15}$$

When the superheat of steam is not considered, the local steam flow rate at the thermocouple elevation, j, is given by

$$W^0_{gj} = W^0_{gj-1} + \frac{q''_j \, \pi D \Delta Z_j}{H_{fg}}, \quad j = 1 \sim 8 . \tag{3-16}$$

The second term in eq. (3-16) indicates the steam generation rate in the section length ΔZ_j. The heat fluxes at the heater tube with 1.3 mm thickness are given by eqs. (3-7) and (3-8). The heat fluxes at the top 20 mm and the bottom 40 mm are higher than the heat flux given by eqs. (3-7) and (3-8) by the factor of 1.27 and 1.57, respectively.

Since the steam is superheated in the present experiment as

discussed in Section 3.5, the actual steam flow rate is given by

$$W_{gj} = W^0_{gj}\left(\frac{x_a}{x_e}\right)_j , \quad j = 1 \sim 8 \tag{3-17}$$

where $(x_a/x_e)_j$ is given by eq. (3-11) or (3-12).

The local water flow rate is given by eq. (3-15) using the total flow rate, W_T, and the steam flow rate, W_{gj}, defined by eq. (3-17).

The superficial steam and water velocities are defined as

$$\left.\begin{aligned} U_{gj} &= \frac{W_{gj}}{S\,\rho_g} , \quad j = 1 \sim 8 \\ U_{\ell j} &= \frac{W_{\ell j}}{S\,\rho_\ell} , \quad j = 1 \sim 8 \end{aligned}\right\} \tag{3-18}$$

where the superheated steam density, ρ_g, is obtained at the superheated temperature, while the liquid density, ρ_ℓ, is obtained at the saturation temperature.

The linear steam and water velocities at the thermocouple elevations are given by

$$\left.\begin{aligned} v_{gj} &= \frac{W_{gj}}{\alpha\, S\rho_g} , \quad j = 1 \sim 8 \\ v_{\ell j} &= \frac{W_{\ell j}}{(1-\alpha)S\,\rho_\ell} , \quad j = 1 \sim 8 \end{aligned}\right\} \tag{3-19}$$

Table 3.1 Test conditions

Geometry	: annulus,	inner diameter	0.0159 m
		outer diameter	0.034 m
		heated length	0.8 m
Flow direction	: vertical upward		
Fluid	: steam-water mixture		
Pressure	: 0.175 $\sim$ 0.38 MPa		
Wall temperature	: 865 $\sim$ 1099 K		
Heat flux	: $0.87 \times 10^5 \sim 1.79 \times 10^5$ W/m^2		
Void fraction	: 0.457 $\sim$ 0.946		
Superficial water velocity	: 0.012 $\sim$ 0.095 m/s		
linear water velocity	: 0.038 $\sim$ 0.71 m/s		
linear steam velocity	: 4.2 $\sim$ 16.5 m/s		

Table 3.2 Experimental ranges used for Chen's correlation

Geometry	: vertical tube
Pressure	: 0.42 $\sim$ 19.5 MPa
Diameter	: 0.00488 $\sim$ 0.020 m
Mass flux	: 16.3 $\sim$ 52.4 kg/m^2 s
Equilibrium quality	: 0.151 $\sim$ 1.728
Heat flux	: $3.38 \times 10^4 \sim 2.05 \times 10^6$ W/ m^2

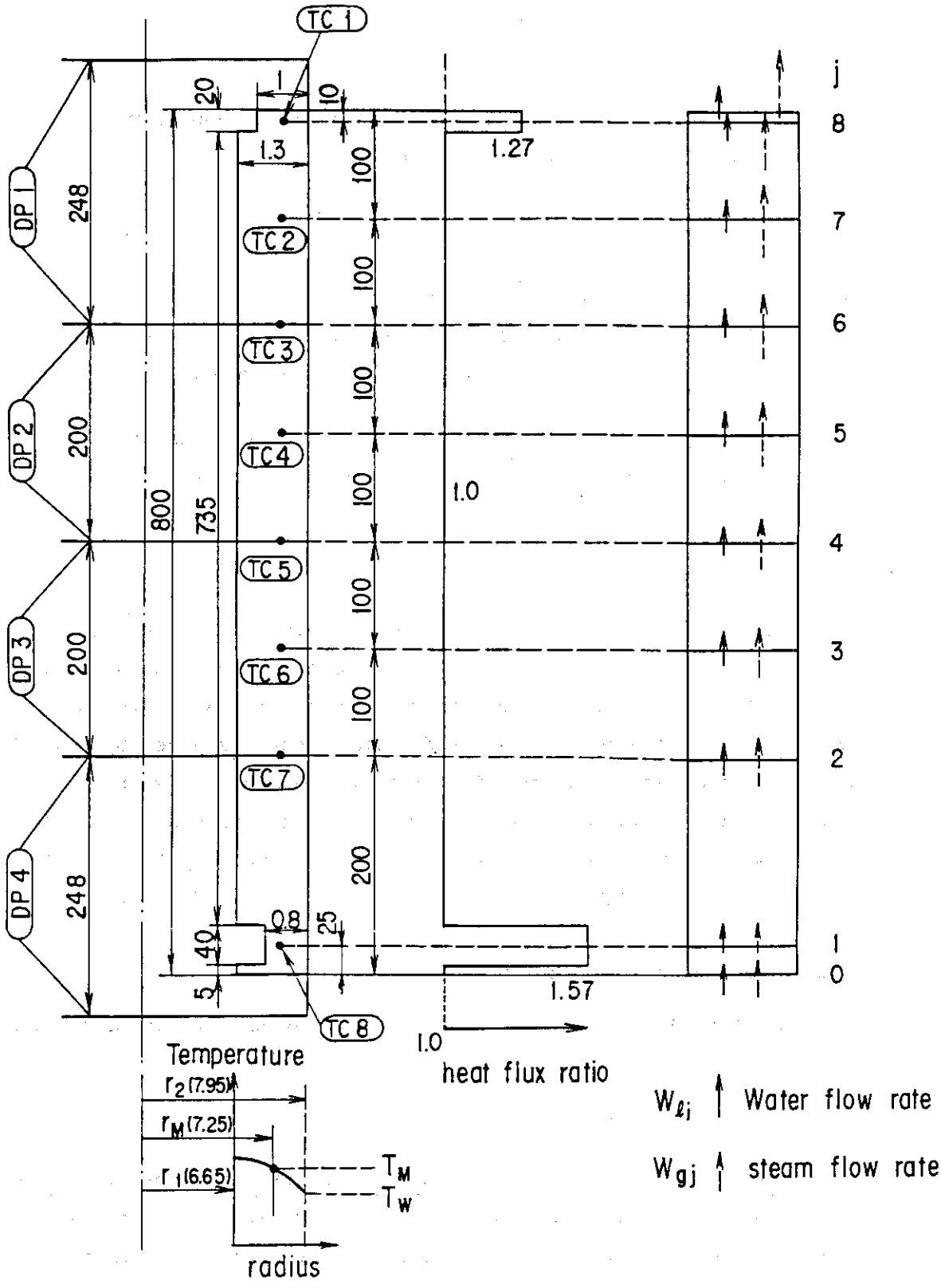

Fig. 3.1 Heater tube geometry and instrumentation

4. Results and Discussions

4.1 Total Heat Flux

The total heat flux from the wall to the two-phase mixture is considered to be a sum of three components;

$$q''_t = q'_r + q''_{FC} + q''_D \tag{4-1}$$

where q''_r = radiation heat flux
q''_{FC} = heat flux due to steam forced convection
q''_D = heat flux due to droplets impingement

The total heat transfer coefficient is defined as the heat transfer coefficient between the wall and the saturated fluid;

$$h_t = \frac{q''_t}{T_w - T_{sat}} \tag{4-2}$$

The measured total heat transfer coefficients are plotted against the liquid fractions and local steam velocities in Figs. 4.1 and 4.2, respectively. The local steam velocities in Fig. 4.2 were obtained under the assumption that the steam temperature is given by eq. (3-13). The total heat transfer coefficient tends to increase with the liquid fraction and the steam velocity. However, the large scatters of data in these figures indicate that a single function of liquid fraction or steam velocity cannot fit the measured heat transfer coefficients.

4.2 Radiation Heat Transfer

The radiation heat flux, q''_r, is given by the Stefan-Boltzmann's law:

$$q''_r = E\,\sigma_{SB}\,(T_w^4 - T_{sat}^4) \tag{4-3}$$

Here, the emissivity of heater rod is assumed to be 0.7. Furthermore, the total amount of the radiation heat flux is assumed to be absorbed in the saturated liquid. Then, the radiation component of the heat transfer coefficient is expressed as

$$h_r = 0.7\,\sigma_{SB}\,(T_w^4 - T_{sat}^4)/(T_w - T_{sat}) \tag{4-4}$$

As shown in Fig. 4.3, the radiation heat transfer coefficients in the present experiment are between 50 and 80 $W/m^2 \cdot K$.

4.3 Steam Forced Convection Heat Transfer

The Dittus-Boelter correlation was used to evaluate the heat flux due to the steam forced convection:

$$q''_{FC} = 0.023 \frac{k_g}{D_e} \left(\frac{\rho_g v_g D_e}{\mu_g} \right)^{0.8} P_{rg}^{0.4} (T_w - T_g) \qquad (4\text{-}5)$$

Since the thermal non-equilibrium should be generally taken into account in the steam forced convection heat transfer mode, the steam velocity, v_g, is given by eq. (3-19) and the superheated steam properties such as k_g, ρ_g, μ_g and P_{rg} are obtained at the film temperature given by eq. (3-14).

Since the heat transfer coefficients in the present experiment are defined as the general form; $q'' = h(T_w - T_{sat})$, the heat transfer coefficient due to forced convection to superheated steam is expressed as

$$h_{FC} = 0.023 \frac{k_g}{D_e} \left(\frac{\rho_g v_g D_e}{\mu_g} \right)^{0.8} P_{rg}^{0.4} \frac{(T_w - T_g)}{(T_w - T_{sat})} \qquad (4\text{-}6)$$

As discussed in Section 3.5, the steam temperature, T_g, in the present experiment is estimated to be between the calculated temperature based on the Chen's model (eq. (3-13)) and the saturation temperature. In order to evaluate the sensitivity of steam temperature on the result, the heat transfer coefficients due to steam forced convection (h_{FC}) are obtained under two extream cases; T_g = eq. (3-13) and $T_g = T_{sat}$, and shown in Figs. 4.4 and 4.5, respectively, against the local steam velocities which are also affected by the steam temperature. The heat transfer coefficients in Fig. 4.5 are higher by approximately 50 % than those in Fig. 4.4. In any cases, the h_{FC} is less than 25 % of the total heat transfer coefficient and occupies the smallest ratio among the three heat transfer components in the present experiment.

4.4 Heat Transfer due to Droplets Impingement

The heat transfer coefficient due to droplets impingement, h_D, is

obtained from eq. (4-1) as

$$h_D = (q''_t - q''_r - q''_{FC})/(T_w - T_{sat}) = h_t - h_r - h_{FC} \tag{4-7}$$

where q''_r and q''_{FC} are evaluated using eqs. (4-3) and (4-5), respectively.

In order to obtain a correlation of h_D as a function of steam and water velocities and liquid fraction (1-void fraction), a Forslund-Rohsenow type equation was used to evaluate the heat transfer from wall to satulated liquid droplets.

Forslund and Rohsenow[8] proposed the following equation for the heat flux from wall to a single layer of droplets next to the surface of the heater rod:

$$q''_D = K_1 K_2 \left(\frac{\pi}{4}\right)\left(\frac{6\ G_t}{\pi\ \rho_\ell}\right)^{\frac{2}{3}}\left(\frac{1 - x_a}{v_\ell}\right)^{\frac{2}{3}}\left(\frac{1}{\delta}\right)^{\frac{1}{4}} \phi(T_w, P) \tag{4-8}$$

where

$$\phi(T_w, P) = \left[\frac{k_g^{\,3}\ H^*_{fg}\ g\ \rho_g\ \rho_\ell}{(T_w - T_{sat})\mu_g(\pi/6)^{\frac{1}{3}}}\right]^{\frac{1}{4}} (T_w - T_{sat})$$

$$H^*_{fg} = H_{fg}\left[1 + \frac{7}{20}\frac{C_{pg}(T_w - T_{sat})}{H_{fg}}\right]^{-3}$$

Using the relation of $G_t(1 - x_a) = \rho_\ell\ v_\ell(1 - \alpha)$, eq. (4-8) can be rewritten as

$$q''_D = K_1 K_2 \left(\frac{\pi}{4}\right)\left(\frac{6}{\pi}\right)^{\frac{2}{3}}\ (1 - \alpha)^{\frac{2}{3}}\left(\frac{1}{\delta}\right)^{\frac{1}{4}} \phi(T_w, P) \tag{4-9}$$

Although eq. (4-9) requests the value of droplet diameter, it is practically difficult to specify the droplet diameter in a dispersed film boiling flow channel. Here the maximum droplet diameter is assumed to be governed by a critical Weber number

$$We = \frac{\rho_g(v_g - v_\ell)^2\delta}{\sigma} \tag{4-10}$$

That is,

$$\delta = \frac{\sigma\ We}{\rho_g(v_g - v_\ell)^2} \tag{4-11}$$

Substituting eq. (4-11) into eq. (4-9), the following correlation of heat transfer coefficient is obtained:

$$h_D = C(1 - \alpha)^{\frac{2}{3}}(v_g - v_\ell)^{\frac{1}{2}}F(T_w,P) \tag{4-12}$$

$$\text{where} \quad C = K_1K_2\left(\frac{\pi}{4}\right)\left(\frac{6}{\pi}\right)^{\frac{2}{3}} \Big/ We^{\frac{1}{4}} \tag{4-13}$$

$$F(T_w,P) = \left[\frac{k_g^3 H_{fg}^* g \rho_g^2 \rho_\ell}{(T_w - T_{sat})\mu_g(\pi/6)^{\frac{1}{3}}\sigma}\right]^{\frac{1}{4}} \tag{4-14}$$

The magnitude of the empirical constant C in eq. (4-12) can be estimated by using the experimental data. However, the h_D obtained from eq. (4-7) depends on the other two heat transfer components; h_r and h_{FC}, which are estimated by eqs. (4-4) and (4-6), respectively. Especially, the maximum uncertainty involved in h_{FC} is approximately 50 % depending on the steam temperature as discussed in Section 3.5. The values of $h_D/\{(v_g-v_\ell)^{\frac{1}{2}}F(T_w,P)\}$ are plotted against $(1 - \alpha)^{\frac{2}{3}}$ in Figs. 4.6 and 4.7 for the cases of T_g = eq. (3-13) and $T_g = T_{sat}$, respectively. As shown in these figures, C = 0.57 and C = 0.9 are appropriate values for correlating the data points in these two extream cases, respectively. In order to find the relation between C and T_g, the values of C are additionally obtained by assuming the steam temperatures between 450 and 650 K and the resultant C values are plotted against $(T_g - T_{sat})/(T_{g,Chen} - T_{sat})$ in Fig. 4.8. The $T_{g.Chen}$ is the average value of steam temperatures calculated from eq. (3-13) and equal to about 720 K in the present experiment. As shown in Fig. 4.8, the value of C can be approximated as 0.6 when the $(T_g - T_{sat})/(T_{g,Chen} - T_{sat})$ is greater than 0.5.

Forslund and Rohsenow assumed the value of K_1K_2 as 0.2 for nitrogen flow and the critical Weber number as 7.5. In this case, the value of C in eq. (4-13) becomes 0.146. This value is much less than the value obtained from eq. (4-12) based on the experimental data in the present experiment.

Figure 4.9 shows the comparison between experimental and calculated heat transfer coefficients due to droplets impingement for the case of $T_g = T_{g.Chen}$ and C = 0.57. The agreement is fairly well within 20 %.

4.5 Observation of Flow Pattern

Photo. 4.1 shows the photographs of flow pattern together with the experimental conditions for each Run. The three photographs for each Run represent the typical flow patterns observed under the same experimental conditions. Since the glass shroud was used for the flow observation test, the differential pressures in the flow channel were not measured and therefore the void fractions, local steam velocities and local water velocities could not be obtained. The local steam and water velocities and the void fractions shown in Photo 4.1 were estimated from the corresponding test results using the stainless steel shroud under approximately the same conditions as in the glass shroud tests.

Based on these photographs and the flow observation with the high speed video camera, the flow pattern in the present film boiling experiment can be classified into three flow regimes by the void fractions:

(1) Void fraction 0.9 ~ 0.95 (Runs 1 and 6)
Dispersed flow
The droplet diameter is relatively small.

(2) Void fraction 0.8 ~ 0.9 (Runs 2 and 8)
Dispersed flow
The droplet diamer is larger than that in case (1).

(3) Void fraction 0.7 ~ 0.8 (Runs 3, 5, 7, 9)
Slug flow

The effects of the steam and water velocities on the flow pattern were not clearly observed in the present experimental ranges.

Run 10 is a special test to see the bottom and top quench fronts on the heater rod.

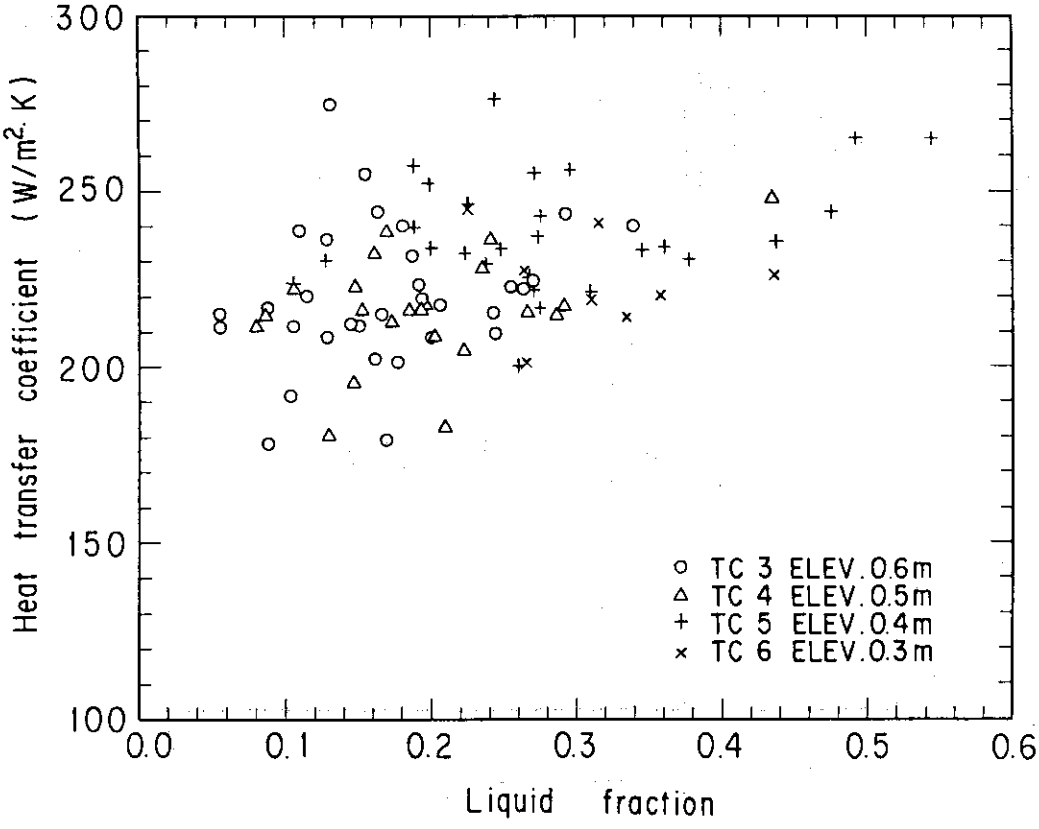

Fig. 4.1 Measured heat transfer coefficient vs. liquid fraction

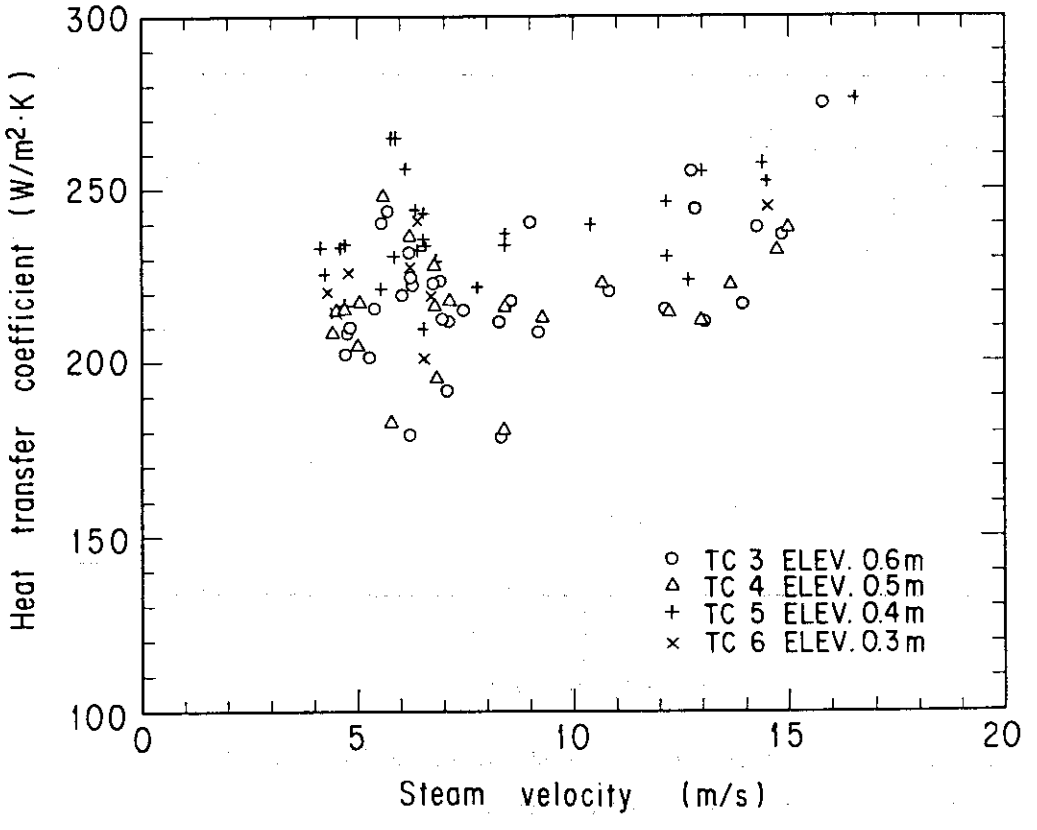

Fig. 4.2 Measured heat transfer coefficient vs. steam velocity

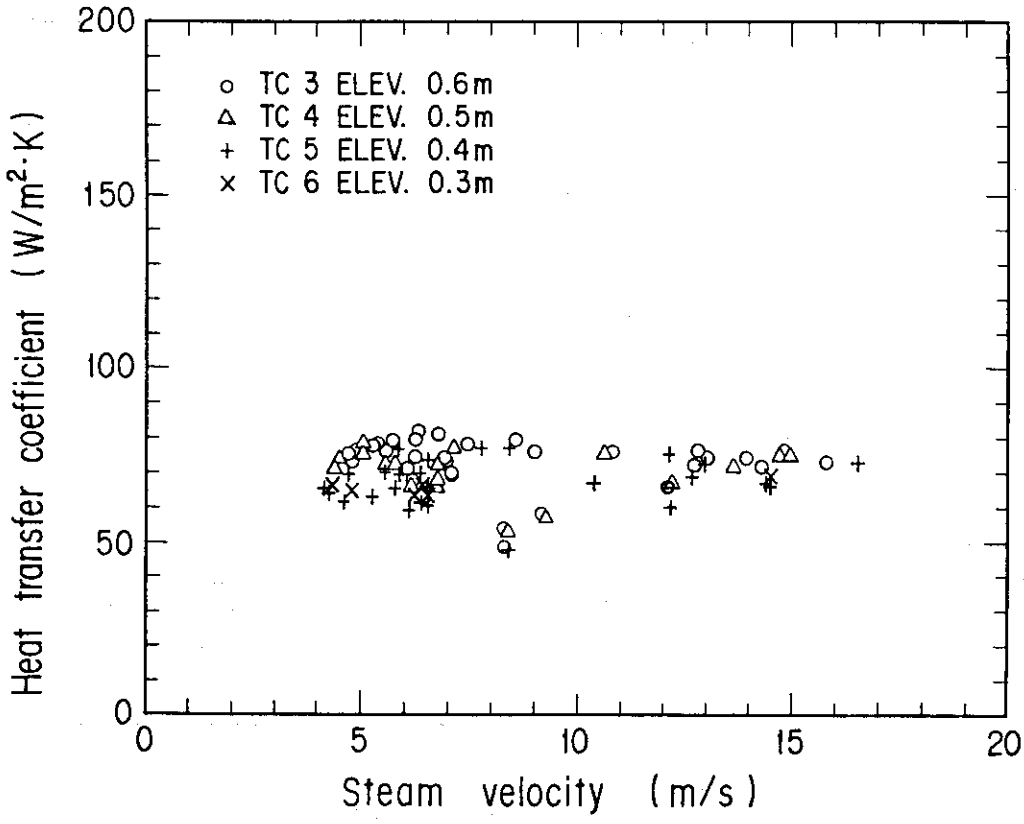

Fig. 4.3 Heat transfer coefficient due to radiation vs. steam velocity (T_g = Chen's model)

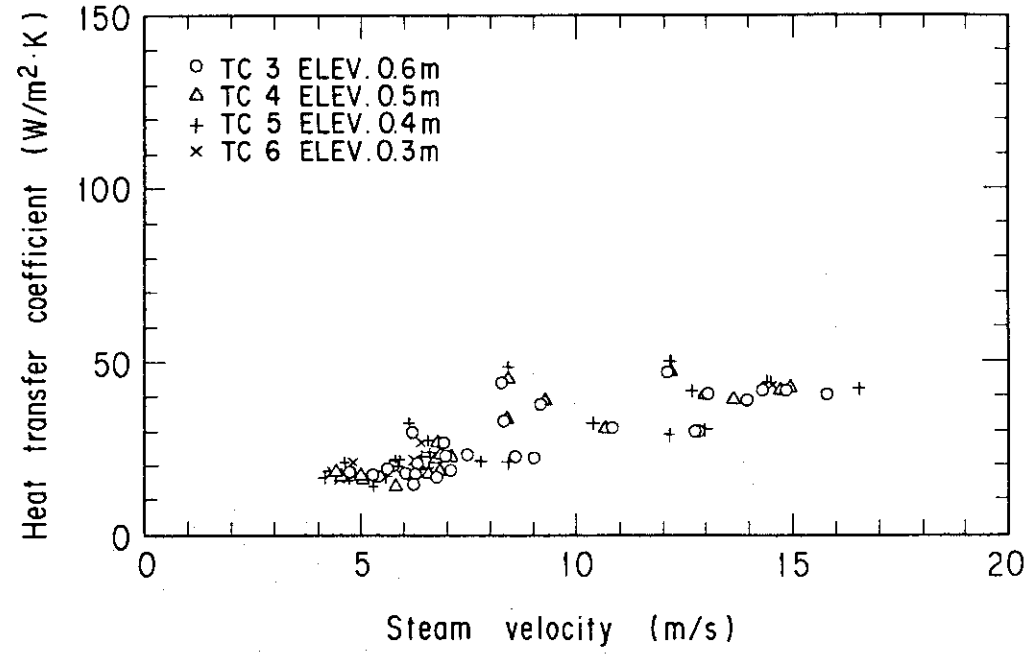

Fig. 4.4 Heat transfer coefficient due to forced convection vs. steam velocity (T_g = Chen's model)

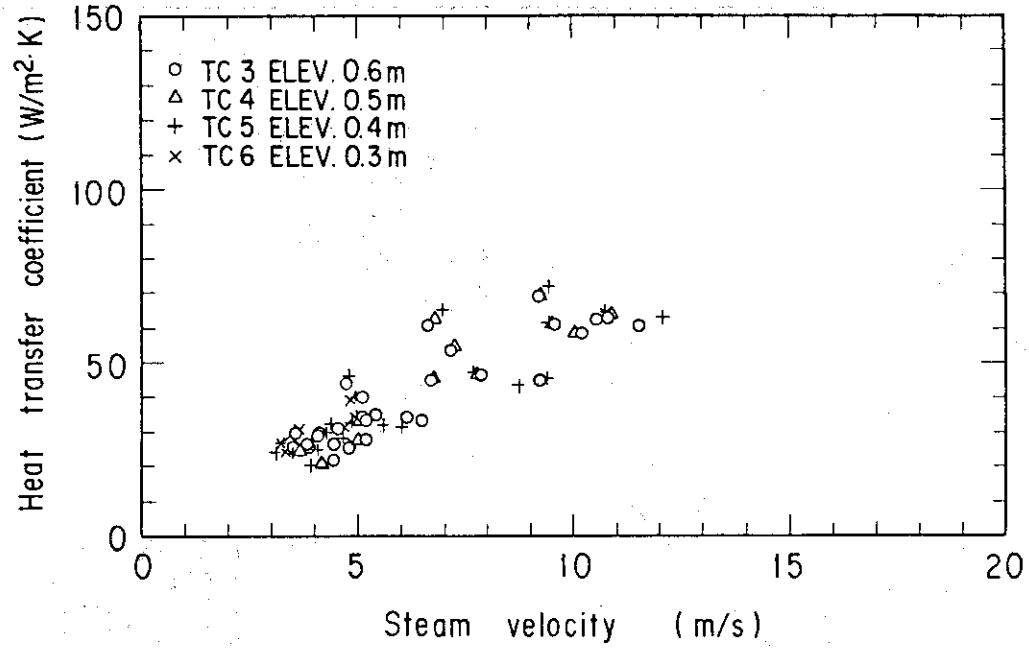

Fig. 4.5 Heat transfer coefficient due to forced convection vs. steam velocity (T_g = saturation temperature)

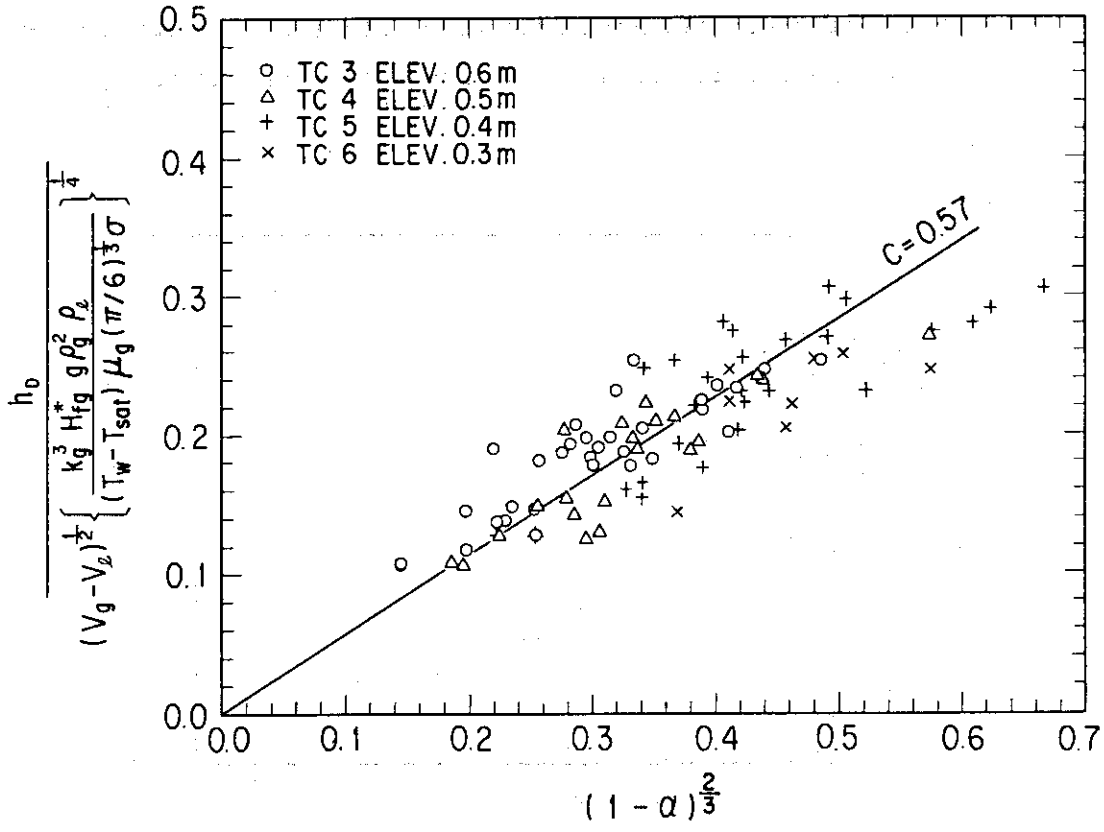

Fig. 4.6 Relation between heat transfer coefficient due to droplets impingement and liquid fraction (T_g = Chen's model)

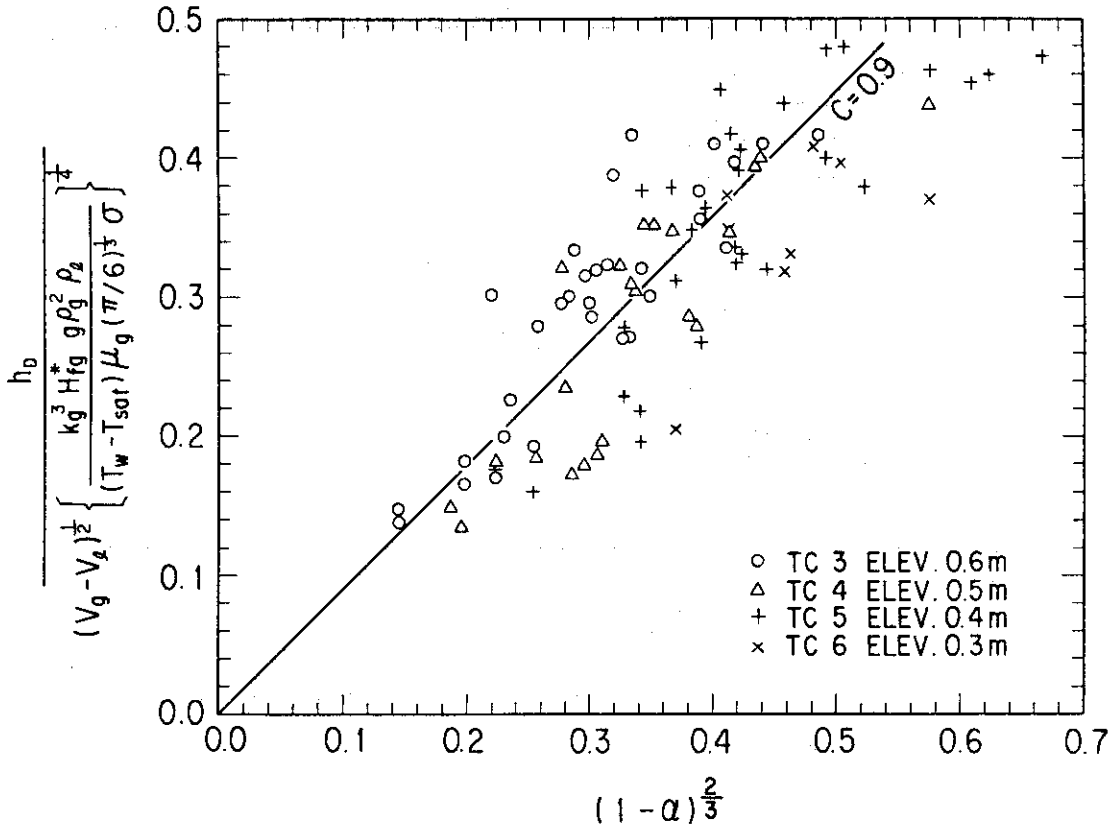

Fig. 4.7 Relation between heat transfer coefficient due to droplets impingement and liquid fraction (T_g = Saturation temperature)

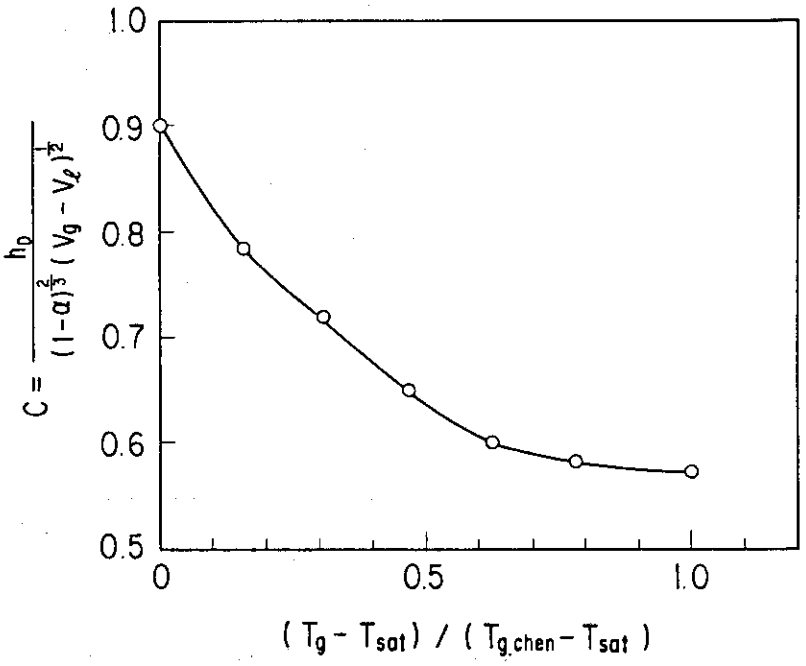

Fig. 4.8 Relation between "$h_D/\{(1-\alpha)^{\frac{2}{3}}(v_g-v_\ell)^{\frac{1}{2}}\}$" and steam temperature

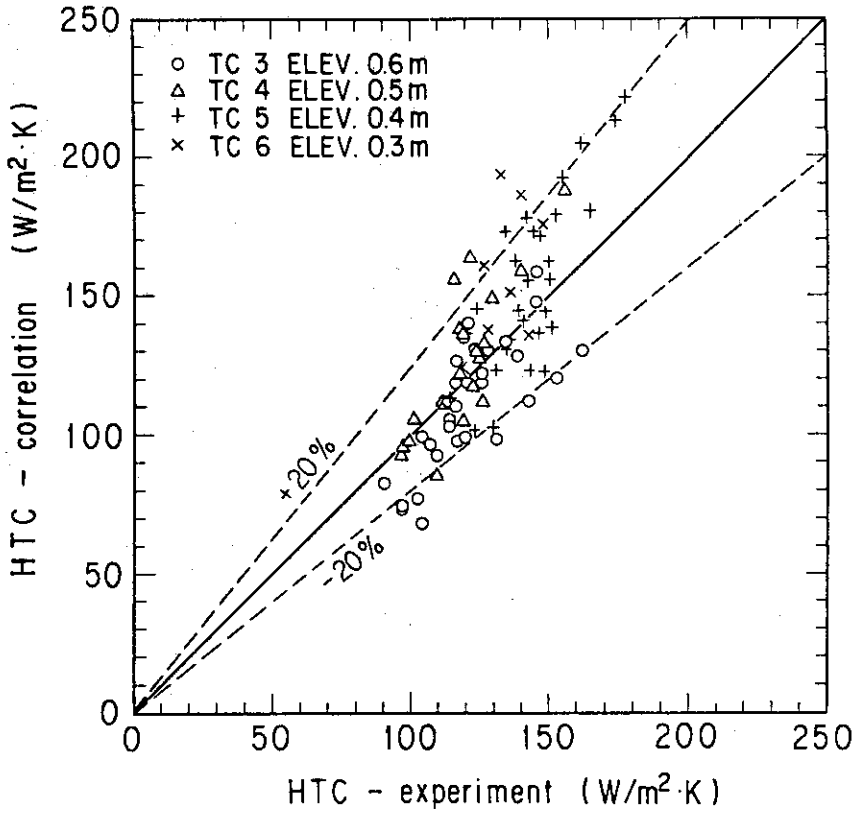

Fig. 4.9 Comparison between correlation and experimental data

Run = 1

Q_ℓ = 1.0 ℓ/min

u_ℓ = 0.022 m/s

Q_g = 300 ℓ/min

P = 0.2 MPa

T_w (TC 3) = 1066 K

T_w (TC 4) = 1052 K

q'' = 1.23×10^5 W/m^2

h_t = 184 W/m^2·K

v_ℓ = 0.3 - 0.45 m/s

v_g = 15.0 - 15.8 m/s

α = 0.9 - 0.95

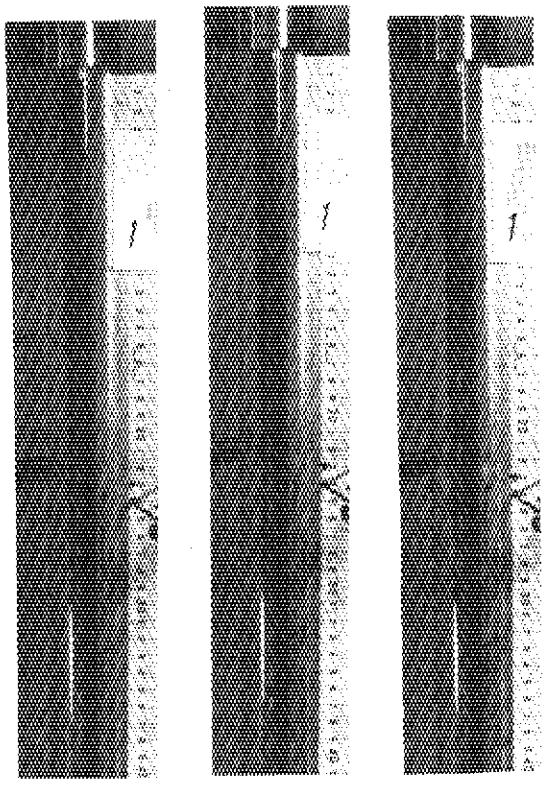

Run = 2

Q_ℓ = 1.0 ℓ/min

u_ℓ = 0.022 m/s

Q_g = 200 ℓ/min

P = 0.2 MPa

T_w (TC 3) = 1057 K

T_w (TC 4) = 1047 K

q'' = 1.17×10^5 W/m^2

h_t = 177 W/m^2·K

v_ℓ = 0.18 - 0.26 m/s

v_g = 10.0 - 10.5 m/s

α = 0.85 - 0.9

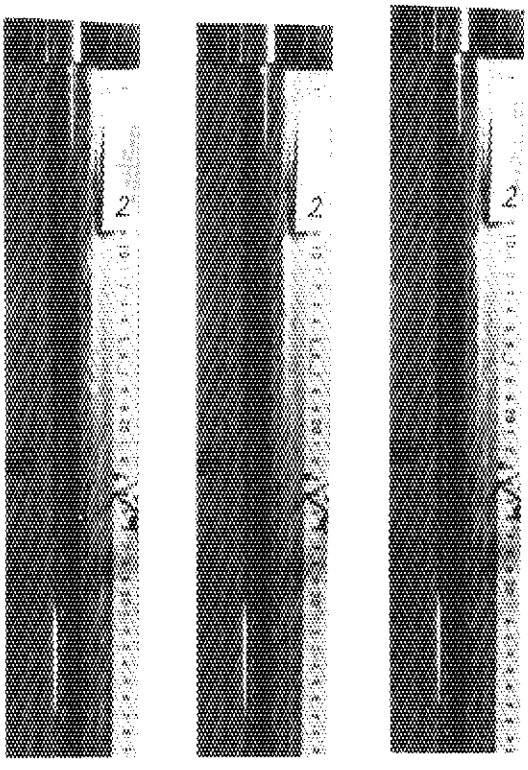

Photo. 4.1 Flow pattern in test section

Run = 3

Q_ℓ = 1.0 ℓ/min

u_ℓ = 0.022 m/s

Q_g = 50 ℓ/min

P = 0.2 MPa

T_w (TC 3) = 1061 K

T_w (TC 4) = 1052 K

q" = 1.21×10^5 W/m^2

h_t = 182 W/m^2·K

v_ℓ = 0.08 - 0.12 m/s

v_g = 5.5 - 6.0 m/s

α = 0.7 - 0.8

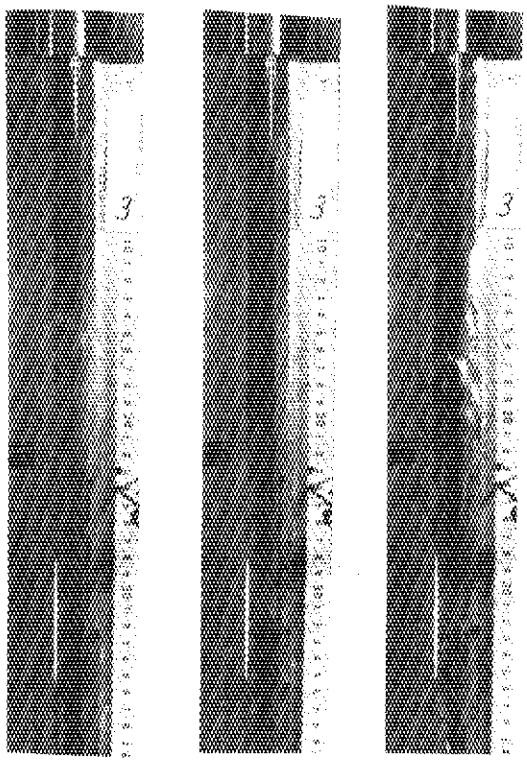

Run = 4

Q_ℓ = 3.0 ℓ/min

u_ℓ = 0.07 m/s

Q_g = 300 ℓ/min

P = 0.25 MPa

T_w (TC 3) = 1057 K

T_w (TC 4) = 1052 K

q" = 1.49×10^5 W/m^2

h_t = 228 W/m^2·K

v_ℓ = unknown

v_g = "

α = "

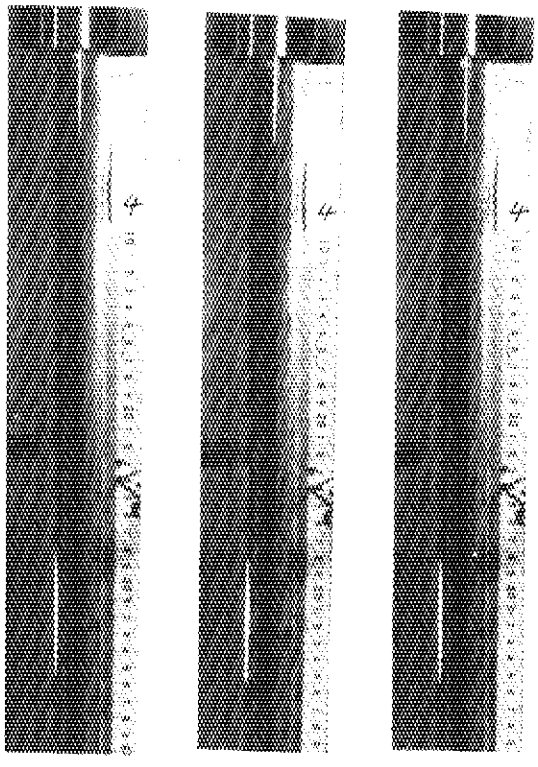

Photo. 4-1 (continue)

Run = 5

Q_ℓ = 3.0 ℓ/min

u_ℓ = 0.07 m/s

Q_g = 50 ℓ/min

P = 0.25 MPa

T_w (TC 3) = 1071 K

T_w (TC 4) = 1059 K

q'' = 1.39×10^5 W/m^2

h_t = 208 W/m^2·K

v_ℓ = 0.18 - 0.26 m/s

v_g = 7.0 - 8.0 m/s

α = 0.7 - 0.75

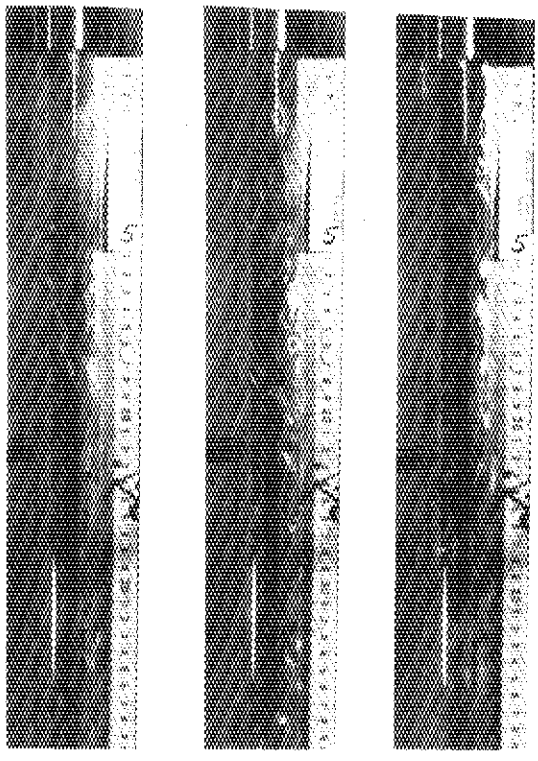

Run = 6

Q_ℓ = 0.6 ℓ/min

u_ℓ = 0.012 m/s

Q_g = 300 ℓ/min

P = 0.25 MPa

T_w (TC 3) = 1061 K

T_w (TC 4) = 1047 K

q'' = 1.30×10^5 W/m^2

h_t = 198 W/m^2·K

v_ℓ = 0.14 - 0.17 m/s

v_g = 16.0 - 17.0 m/s

α = 0.9 - 0.95

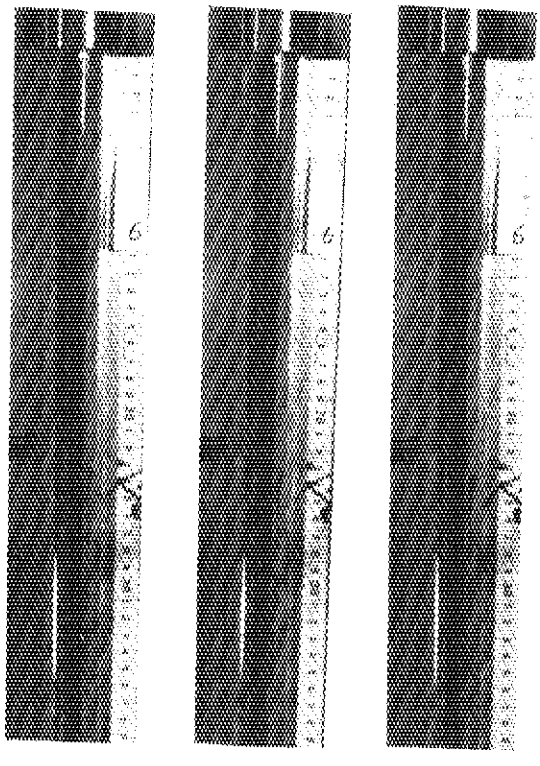

Photo. 4-1 (continue)

Run = 7

Q_ℓ = 0.7 ℓ/min

u_ℓ = 0.012 m/s

Q_g = 50 ℓ/min

P = 0.25 MPa

T_w (TC 3) = 1042 K

T_w (TC 4) = 1038 K

q'' = 1.23×10^5 W/m^2

h_t = 192 W/m^2·K

v_ℓ = 0.05 - 0.08 m/s

v_g = 5.2 - 6.0 m/s

α = 0.75 - 0.85

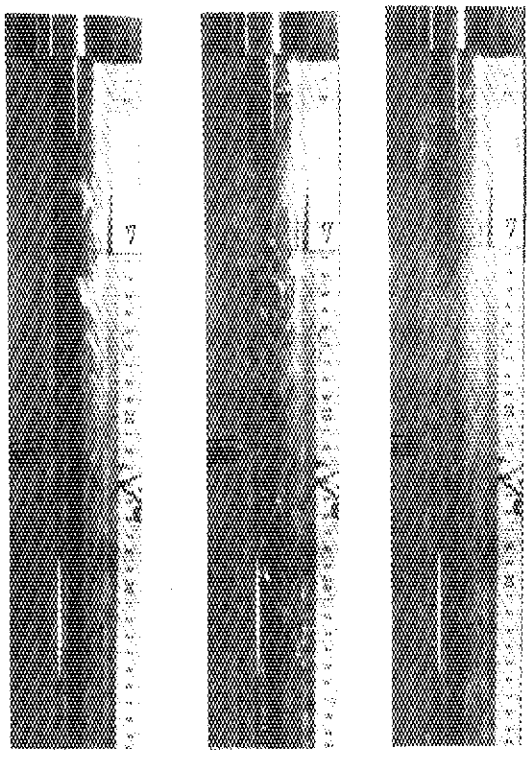

Run = 8

Q_ℓ = 2.0 ℓ/min

u_ℓ = 0.045 m/s

Q_g = 300 ℓ/min

P = 0.25 MPa

T_w (TC 3) = 1066 K

T_w (TC 4) = 1066 K

q'' = 1.46×10^5 W/m^2

h_t = 220 W/m^2·K

v_ℓ = 0.24 - 0.43 m/s

v_g = 17.3 - 18.0 m/s

α = 0.8 - 0.9

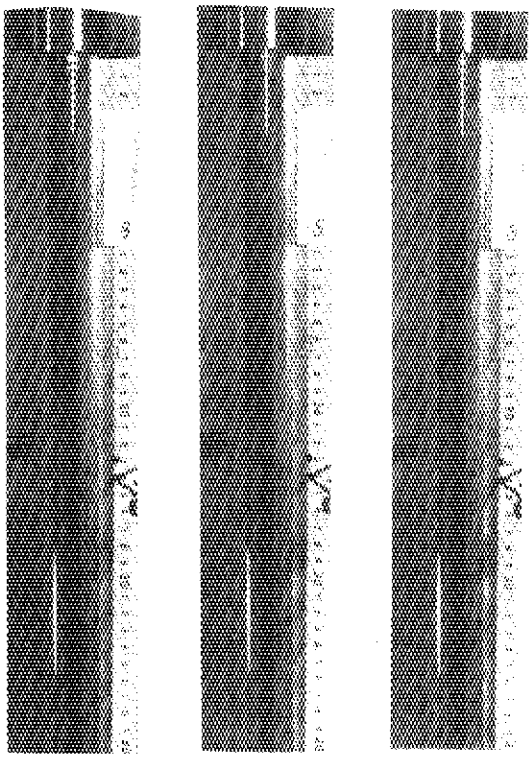

Photo. 4-1 (continue)

Run = 9

Q_ℓ = 2.0 ℓ/min

u_ℓ = 0.045 m/s

Q_g = 50 ℓ/min

P = 0.3 MPa

T_w (TC 3) = 1081 K

T_w (TC 4) = 1071 K

q" = 1.38×10^5 W/m^2

h_t = 205 W/m^2·K

v_ℓ = 0.2 - 0.3 m/s

v_g = 6.5 - 7.5 m/s

α = 0.75 - 0.85

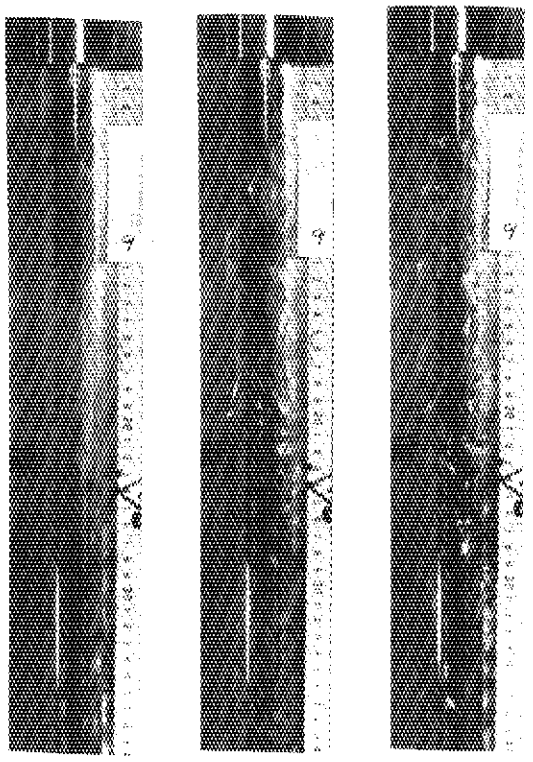

Run = 10

Q_ℓ = 2.0 ℓ/min

u_ℓ = 0.045 m/s

Q_g = 50 ℓ/min

P = 0.3 MPa

T_w (TC 3) = 1076 K

T_w (TC 4) = 1028 K

q" = 1.31×10^5 W/m^2

h_t = 196 W/m^2·K

v_ℓ = 0.2 - 0.3 m/s

v_g = 6.5 - 7.5 m/s

α = 0.75 - 0.85

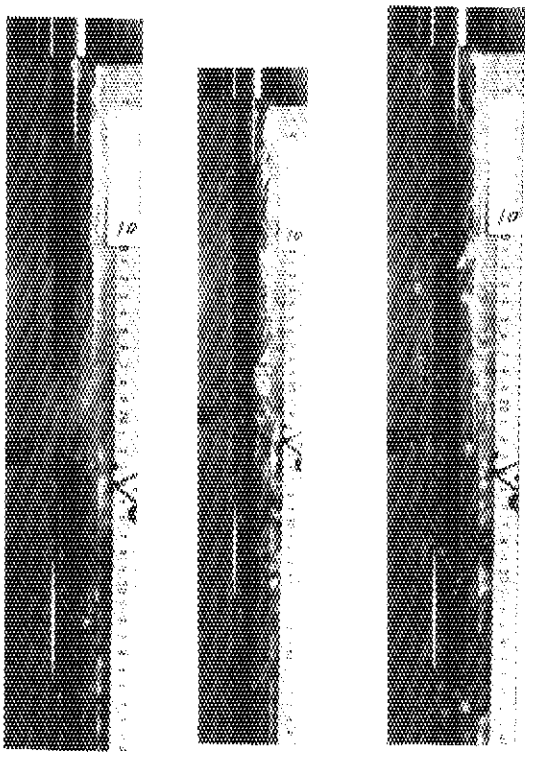

Photo. 4-1 (continue)

5. Conclusion

In order to investigate the relation between film boiling heat transfer coefficient and local flow parameters such as steam and water velocities and void fraction, a steady-state film boiling experiment was performed. The film boiling heat transfer was assumed to be superimposed by three different mechanisms; radiation, forced convection to steam and droplet impingement on wall. The radiation and forced convection heat transfer coefficients were evaluated by using the Stefan-Boltzmann equation and the Dittus-Boelter equation, respectively. The thermodynamic non-equilibrium was taken into account in the forced convection heat transfer mode.

A new correlation for the heat transfer coefficient due to droplet impingement was derived from the dispersed flow heat transfer model developed by Forslund and Rohsenow. The correlation is a function of steam and water velocities, void fraction, fluid properties and wall superheat as given by

$$h_D = C(1 - \alpha)^{\frac{2}{3}}(v_g - v_\ell)^{\frac{1}{2}}F(T_w,P)$$

where

$$F(T_w,P) = \left[\frac{k_g^3 H_{fg}^* g \rho_g^2 \rho_\ell}{(T_w - T_{sat})\mu_g(\pi/6)^{\frac{1}{3}}\sigma}\right]^{\frac{1}{4}}$$

$$H_{fg}^* = H_{fg}\left[1 + \frac{7}{20}\frac{C_{pg}(T_w - T_{sat})}{H_{fg}}\right]^{-3}$$

The value of "C" is a constant depending on steam temperature. The "C" was estimated to be 0.57 if the superheated steam temperature could be calculated from the Chen's semi-empirical correlation.

The agreement between calculated and experimentally derived heat transfer coefficients was fairly good for the present experiment.

Acknowledgment

The author is much indebted to Dr. Y. Murao for his guidance and encouragement for this program.

He would like to express his appreciation to Mr. H. Adachi for his usefull discussion and to Mr. Zhang Boyi from Southwest Reactor Engineering Research and Design Center, China, for his devoted contribution to the present study.

Nomenclature

a	:	thermal diffusivity
B_i	:	Biot number
$B(P)$	:	Correlation in eq. (3-11)
C	:	constant in eq. (4-12)
c_{pg}	:	Specific heat of steam
D	:	diameter of heater rod
De	:	hydraulic equivalent diameter
E	:	emissivity
$F(T_w,P)$	:	function defined in eq. (4-14)
F_o	:	Fourier number
G_t	:	total mass velocity
g	:	acceleration due to gravity
H	:	enthalpy
H_{fg}	:	latent heat of evaporation
h	:	heat transfer coefficient
I	:	Current
k	:	thermal conductivity
K_1K_2	:	constant used in eq. (4-8)
L_i	:	measurement span of differential pressure
ℓ	:	heater tube thickness
P	:	pressure
P_c	:	critical pressure
ΔP	:	differential pressure
P_r	:	Prandtle number
q''	:	heat flux
q'''	:	heat generation rate
r	:	radius
r_1	:	heater tube inner radius
r_2	:	heater tube outer radius
S	:	flow area
T	:	temperature
t	:	time
U	:	superficial velocity
V	:	voltage
v	:	velocity

W : mass flow rate
Xa : actual quality
Xe : equilibrium quality
ΔZ : section length

Greek

α : void fraction
δ : droplet diameter
μ : viscosity
ρ : density
σ : surface tension
σ_{SB} : Stefan-Boltzmann constant
ϕ : function defined in eq. (4-8)

Subscripts

D : droplets impingement
FC : forced convection to steam
f : steam film in thermal boundary layer
g : steam
ℓ : liquid
M : measured
r : radiation
sat : saturation
t : total
W : wall

References

(1) J.C. Chen et al., A Phenomenological Correlation for Post-CHF Heat Transfer, NUREG-0237 (1977).

(2) Y. Murao and J. Sugimoto, Correlation of Heat Transfer Coefficient for Saturated Film Boiling during Reflood Phase Prior to Quenching, J. Nucl. Sci. Tech. vol. 18, No. 4, pp 275 ~ 284 (1981).

(3) Y. Murao et al., REFLA-1D/Mode 3: A Computer Code for Reflood Thermo-Hydrodynamic Analysis during PWR-LOCA -User's Manual-, JAERI-M 84-243 (1985).

(4) M.J. Thurgood et al., COBRA/TRAC - A Thermal-Hydraulics Code for Transient Analysis of Nuclear Reactor Vessels and Primary Coolant Systems, NUREG/CR-3046 (1983).

(5) T. Iwamura et al., Two-Dimensional Thermal-Hydraulic Behavior in Core in SCTF Core-II Cold Leg Injection Tests (Radial Power Profile Test Results), JAERI-M 85-106 (1985).

(6) T. Iwamura and T. Kuroyanagi, Burnout Characteristics under Flow Reduction Condition, J. Nucl. Sci. Tech. vol. 19, No. 6, pp 438 ~ 448 (1982).

(7) M.P. Heisler, Trans. ASME, 69, 227 (1947).

(8) R.P. Forslund and W.M. Rohsenow, Dispersed Flow Film Boiling, J. Heat Transfer, pp 399 - 407, Nov. (1968).